1714

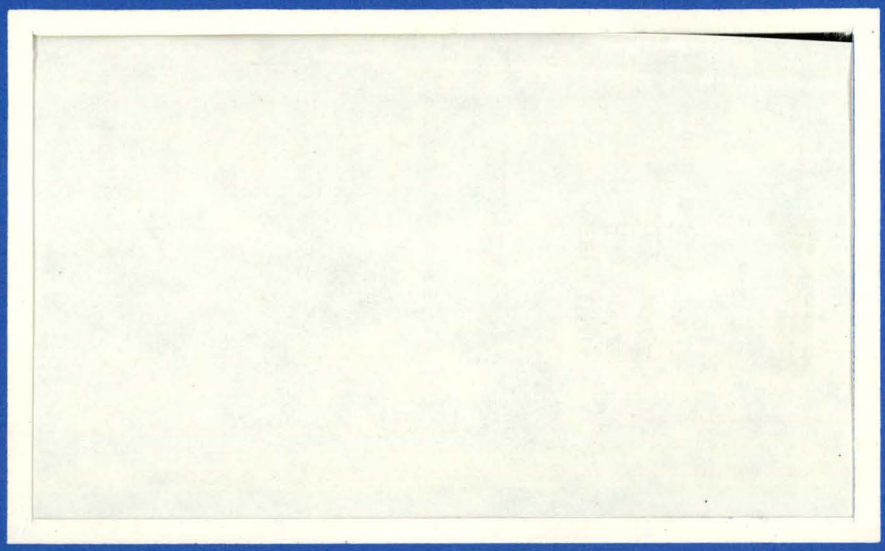

WADCO
CORPORATION
a subsidiary of Westinghouse Electric Corporation
Post Office Box 1970
Richland, Washington 99352

P8532

DISCLAIMER

[redacted]

[redacted] NOTICE

HANFORD ENGINEERING DEVELOPMENT LABORATORY

Richland, Washington
operated by

WADCO CORPORATION

A Subsidiary of Westinghouse Electric Corporation
for the
United States Atomic Energy Commission Under Contract No. AT(45-1)-2170

WHAN-FR-24

UC-25, Metals,
Ceramics, and Materials

IRRADIATION OF BORON CARBIDE PELLETS AND POWDERS IN HANFORD THERMAL REACTORS

December 1970

A. L. Pitner
G. E. Russcher

WADCO CORPORATION
Richland, Washington 99352

UNCLASSIFIED

Printed in the United States of America
Available from
National Technical Information Service
National Bureau of Standards,
U.S. Department of Commerce
Springfield, Virginia 22151
Price: Printed Copy $3.00; Microfiche $0.65

CONTENTS

LIST OF FIGURES

LIST OF TABLES

IRRADIATION OF BORON CARBIDE PELLETS AND POWDERS IN HANFORD THERMAL REACTORS

A. L. Pitner and G. E. Russcher

INTRODUCTION

Boron carbide has been used extensively as a control material in thermal reactors, and its nuclear properties make it an attractive choice for similar fast reactor applications. A serious consideration related to its use in this capacity, however, is the fact that the high operating temperatures required in LMFBR applications may decrease its overall utility by limiting its effective lifetime.

Since it undergoes $^{10}B(n,\alpha)^{7}Li$ capture reactions, the irradiation behavior of boron carbide is characterized by gas release and swelling phenomena similar to those exhibited by ceramic fuels. Previously reported data (1-5) on its performance in thermal reactors have been obtained, for the most part, in the MTR, ETR, and NRU at temperatures below 750°F. These data differ considerably for similar conditions of irradiation temperature and boron burnup, and their inconsistency requires that the applicability of boron carbide for fast reactor service be evaluated only after suitable high temperature, hard spectrum irradiation tests have been conducted.

This experiment was performed as the initial screening test to obtain information on the behavior of boron carbide in the temperature range of interest for fast reactor applications. It was conducted in thermal reactors in order to take advantage of the high thermal neutron absorption cross section of ^{10}B and thus obtain high burnup levels in the shortest possible time. In order to ensure that the data could be applied to a wide variety of potential control rod designs, several types of pellets and powders were irradiated. The conceptual FTR control rod design was used to select specimen temperatures and exposure levels.

A one neutron energy group analysis was performed to provide information on the effect of Hanford irradiations in various samples at different ^{10}B burnup levels. The same techniques were applied to determine the effect of sample geometries. A further extension was a study of other thermal reactors used in generating previously reported data. Thus this report also includes some analysis of irradiation conditions in ETR and NRU. This one group analysis is a predecessor of a more detailed multi energy group analysis now underway. While preliminary in nature, this one group analysis did provide valid qualitative conclusions.

SUMMARY

Natural boron carbide pellets and powders were irradiated in Hanford thermal production reactors at 500-1200°F to a maximum average ^{10}B burnup of 18% ($\sim 26 \times 10^{20}$ captures/cc). Sample forms were 65, 80, and 99% TD pellets and 60 and 80% TD powders. Calculations of exposure conditions for these specimens have shown significant differences in their ^{10}B depletion profiles. The high density materials exhibit greater peak-to-average burnup ratios due to self shielding. The boron burnup analysis has been substantiated by observed differences in microstructures of the irradiated pellets. Metallographic examination disclosed that 99% TD pellets suffered severe damage near the surface but appeared unreacted in the inner core. The 65 and 80% TD pellets experienced radial cracking with no apparent "skin" burnup effect.

Powders exhibited the highest gas release rates, increasing from $\sim$10% at 500°F to $\sim$30% at 850°F. Intermediate density pellets (65 and 80% TD) released less gas than the powders. The 99% TD pellets released less gas than any of the other samples ranging from about 5% at 500°F to $\sim$20% at 1200°F. Gas release in the pellets increased rapidly as the irradiation temperature exceeds 1000°F.

An analysis of exposure conditions for the specimens tested during this experiment and those irradiated in other thermal reactors indicated that spectral differences and sample geometry must be considered when evaluating the irradiation behavior of boron carbide.

MATERIALS

All boron carbide contained natural boron (19.78% ^{10}B). Overall sample dimensions in each capsule were nominally 0.25 inch diameter x 1 inch long. Loose-packed powder (60% TD) was tested as well as powder vibrationally compacted to 80% TD. A mixture of four different particle size ranges was used to formulate the powder samples. The mixing formula and composition of the various particle sizes are given in Table I.

TABLE I

CHARACTERIZATION OF B_4C POWDERS

B and C Analysis: (% by wt.)

Mesh	% of Mix	B	C (Total)	C (Free)	B:C Ratio (Combined)
-325	(24)	77.6	24.0	2.0	3.9
200-325	(21)	77.0	23.4	0.6	3.8
30-60	(10)	78.7	22.1	1.6	4.3
10-20	(45)	68.2	25.0	2.3	3.3

Impurities: (wt%)

Element	-10 +20 mesh	-30 +60 mesh	200 -325 mesh	-325 mesh
Al	0.02	0.05	0.02	0.02
Ca	0.05	0.05	0.05	0.1
Cr	0.001	0.001	0.001	0.001
Cu	0.005	0.01	0.005	0.01
Fe	0.2	0.5	0.2	0.1
Ga	0.002	0.002	0.002	0.002
Mg	0.002	0.002	0.01	0.05
Mn	0.001	0.005	0.001	0.001
Ni	0.005	0.005	0.005	0.005
Pb	0.002	0.002	0.002	0.002
Pt	0.005	0.005	0.005	0.005
Si	0.05	0.05	0.5	0.5
Sn	0.005	0.01	0.005	0.01
Ti	0.005	0.01	0.005	0.01
V	0.005	0.02	--	--

Figure 1 shows a micrograph of several powder particles. In large sizes, there is a great deal of particle-to-particle variation. Many particles have precipitated graphite flakes and some have metallic inclusions which are principally iron. Porosity within a particle varies from zero to perhaps 30%. Much of the porosity is spherical and not surface-connected. This could be a result of impurity volatilization or it could have been caused by stoichiometry variations such as those reported by ORNL (6). Smaller particles are generally more dense and contain less flake graphite. Although the analysis for free carbon shows little difference between large and small particle sizes, this is probably due to small graphite flakes being mixed with the smaller B_4C particles rather than being contained within them.

Three densities of pellets were irradiated: 65, 80, and 99% TD. All were obtained from commercial sources, and they were ground to right circular cylinders prior to irradiation. The composition and porosity distribution of the pellets are given in Table II. The microstructure of 65 and 80% TD pellets is shown in Figures 2 and 3, respectively. These pellets were hot pressed from a relatively coarse feed stock containing many 30-40μ particles. No grain growth occurred in these pellets during hot pressing. Bonding between particles is accomplished only where surfaces in contact have welded together. The difference in density is readily apparent in comparing Figures 2 and 3. As indicated in Table II, the porosity present is primarily surface connected. Second phase particles of Fe, Cr, and Ni (probably stainless steel) have been identified in these pellets, and they are distributed uniformly throughout the material. The pellets showed no pronounced density variation throughout their length, probably because of the low L/D ratio (∿1.0) and the low sinterability of the large-grain feed stock. The microstructure of 99% TD pellets is shown in Figure 4. No metallic second-phase particles could be detected here.

FIGURE 1. PREIRRADIATION B_4C PARTICLES. POLARIZED LIGHT. 32X

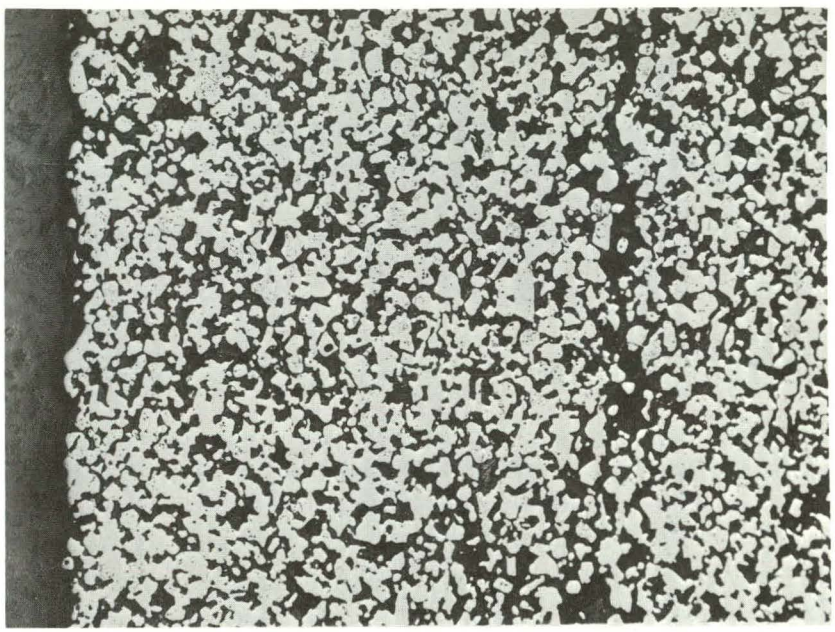

FIGURE 2. MICROSTRUCTURE OF 65% TD PELLET. 80X

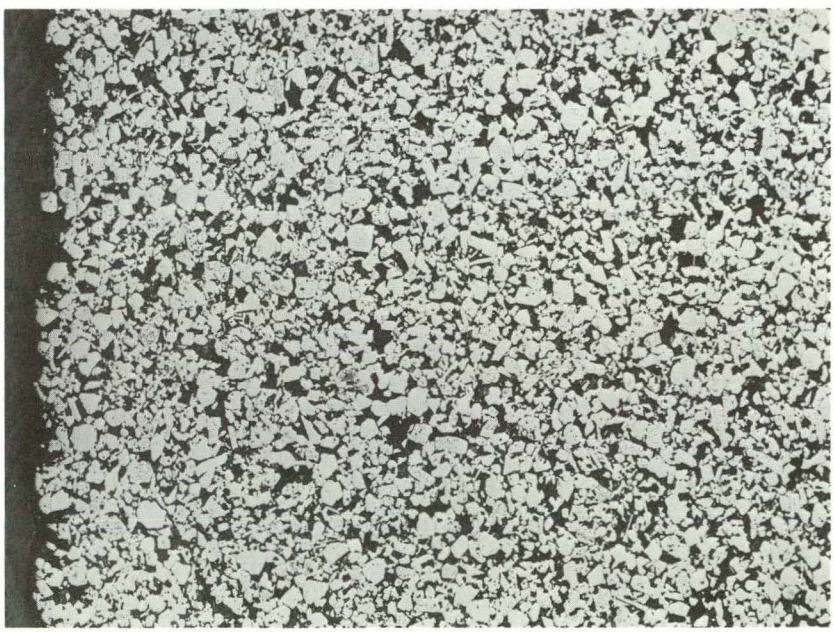

FIGURE 3. MICROSTRUCTURE OF 80% TD PELLET. 80X

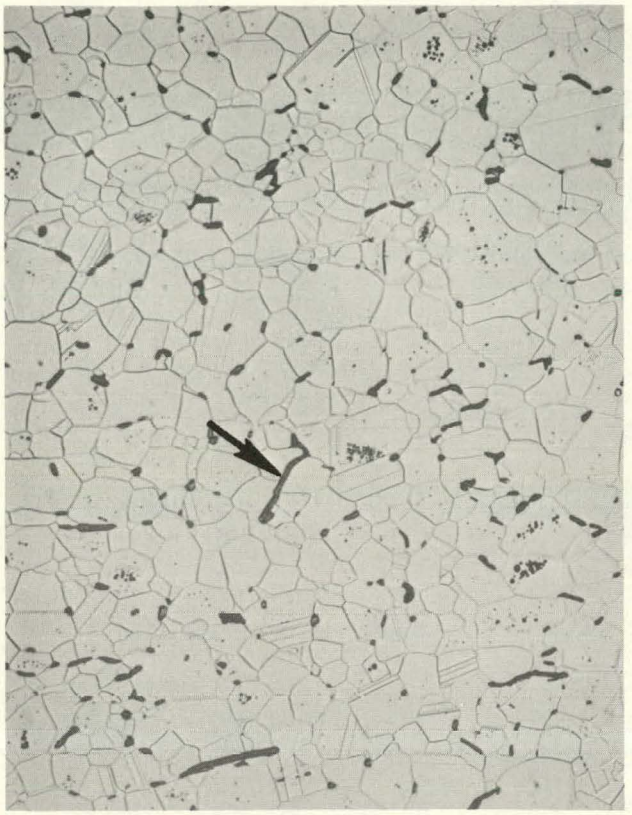

FIGURE 4. MICROSTRUCTURE OF 99% TD PELLET. ARROW INDICATES GRAPHITE PARTICLE. ETCHED IN 10% OXALIC ACID. 275X

TABLE II

CHARACTERIZATION OF HOT-PRESSED B_4C PELLETS

B and C Analysis: (% by wt.)

	B	C (Total)	C (Free)	B:C Ratio (Combined)
65% T.D.	74.9	21.5	0.6	4.0
80-90% T.D.	72.8	21.3	1.0	4.0
99% T.D.	75.6	24.3	0.7	3.6

Impurities: (wt%)

	65% T.D.	80-90% T.D.	99% T.D.
Al	0.02	0.1	0.01
Ca	0.002	0.002	0.002
Cr	0.2	0.1	0.001
Cu	0.05	0.005	0.005
Fe	2.0	0.5	0.05
Ga	<0.002	<0.002	<0.002
Mg	<0.002	0.005	<0.002
Mn	0.005	0.005	<0.005
Nb	<0.005	<0.005	<0.005
Ni	0.5	0.02	--
Si	0.5	0.5	0.1
Sn	0.002	0.002	<0.001
Ti	0.02	0.01	--
V	0.02	<0.005	<0.005

Porosity and Density:

% T.D. (Nominal)	% T.D. (Measured)	% Closed Pores	% Open Pores
65	66.3	1.44	32.23
80	77.0	3.03	19.97
99	99.0	1.0	0

The elongated dark areas (arrow) seen in the micrograph are graphite particles. Small equiaxed dark areas are voids. Average grain size in the 99% TD pellets as determined by random-line intercept techniques (uncorrected) is 14 microns.

EXPERIMENTAL

The irradiation testing was conducted in the Hanford KE and KW production reactors. A test capsule was irradiated initially to establish heating rates in the B_4C and verify capsule operability. The assembly in KW reactor operated at 500-700°F, while the KE assembly operated at 600-1200°F. Each assembly was composed of three subassemblies in tandem that could be discharged separately to provide different exposure levels. Each subassembly contained fifteen capsules, five of which were monitored by chromel-alumel thermocouples. Consequently there were a total of ninety sample irradiations.

In order to determine burnup levels and reaction profiles in individual specimens, the ^{10}B atom density distributions were calculated for three different boron carbide densities as a function of neutron fluence. Burnup calculations were made for boron carbide of theoretical density, 2.52 g/cm, 80% TD and 65% TD for fluences ranging from 5×10^{19} to 1×10^{22} n/cm^2. These represent the nominal densities of the specimens and the exposure range of these experiments.

The average burnup of ^{10}B atoms within an irradiation specimen can be determined from the ^{10}B distribution as a function of depth within the sample. That distribution was calculated as a function of fluence with a computer program developed for these studies.

Self shielding in these cylinders was calculated by an extension of the methods described by Reference (7). In these calculations the effect of neutron self shielding is represented by two semi-cylindrical shielding kernels. One represents attenuation of the fluence from the closest surface of the cylinder, the other represents the attenuation of the fluence originating at the back surface of the cylinder. The radius of the first semi-cylinder is equal to the depth (d) at which the burnup is being calculated. The radius of the second cylinder is equal to D-d, where D is the diameter of the cylinder, or the distance from that point to the back

surface of the specimen. The radii are illustrated in Figure 5. This self-shielding model leads to an approximation which lies between the maximum and minimum self shielding estimates developed by Rockwell (7).

The computational techniques used in this analysis are described in detail in a separate report under preparation (8). A key parameter of this analysis is the ^{10}B neutron capture density as a function of depth in the sample and of neutron fluence. The ^{10}B atom density at each depth of 500 spatial positions is calculated after each increment of fluence. The resultant ^{10}B distribution then determines a new attenuation for that layer of the absorber. The cylindrical self shielding kernels are evaluated with the exponential integral functions tabulated by Rockwell (7) after each fluence increment with the new set of attenuation coefficients for the absorber.

The burnup of ^{10}B in each cylindrical shell (BU_i) is calculated from the ^{10}B atom density. An average burnup ($\overline{BU}$) for the entire specimen is determined with the following relationship, where $r_i = R_o$ at $i = 0$:

$$\overline{BU} = \frac{1}{R_o^2} \sum_{i=1}^{500} BU_i(r^2_{i-1} - r^2_i).$$

These computer calculations produced an almost continuous ^{10}B atom distribution and a reasonable description of the neutron fluence attenuation in the absorber.

In Figure 6, summarized results show average ^{10}B burnup in cylindrical specimens as a function of the total neutron fluence. The relationship between local burnup (BU_i) profile and the specimen averaged burnup are shown in Figure 7 (and Table III) for typical B_4C specimen densities, over a wide fluence range.

Burnup in powdered specimens of subassemblies 1, 2, and 4 were measured by mass spectroscopic analysis of the $^{10}B/^{11}B$ ratio. These data established the relationship between irradiation exposure and average ^{10}B burnup for the specimens. With this experimentally determined relationship, fluences were

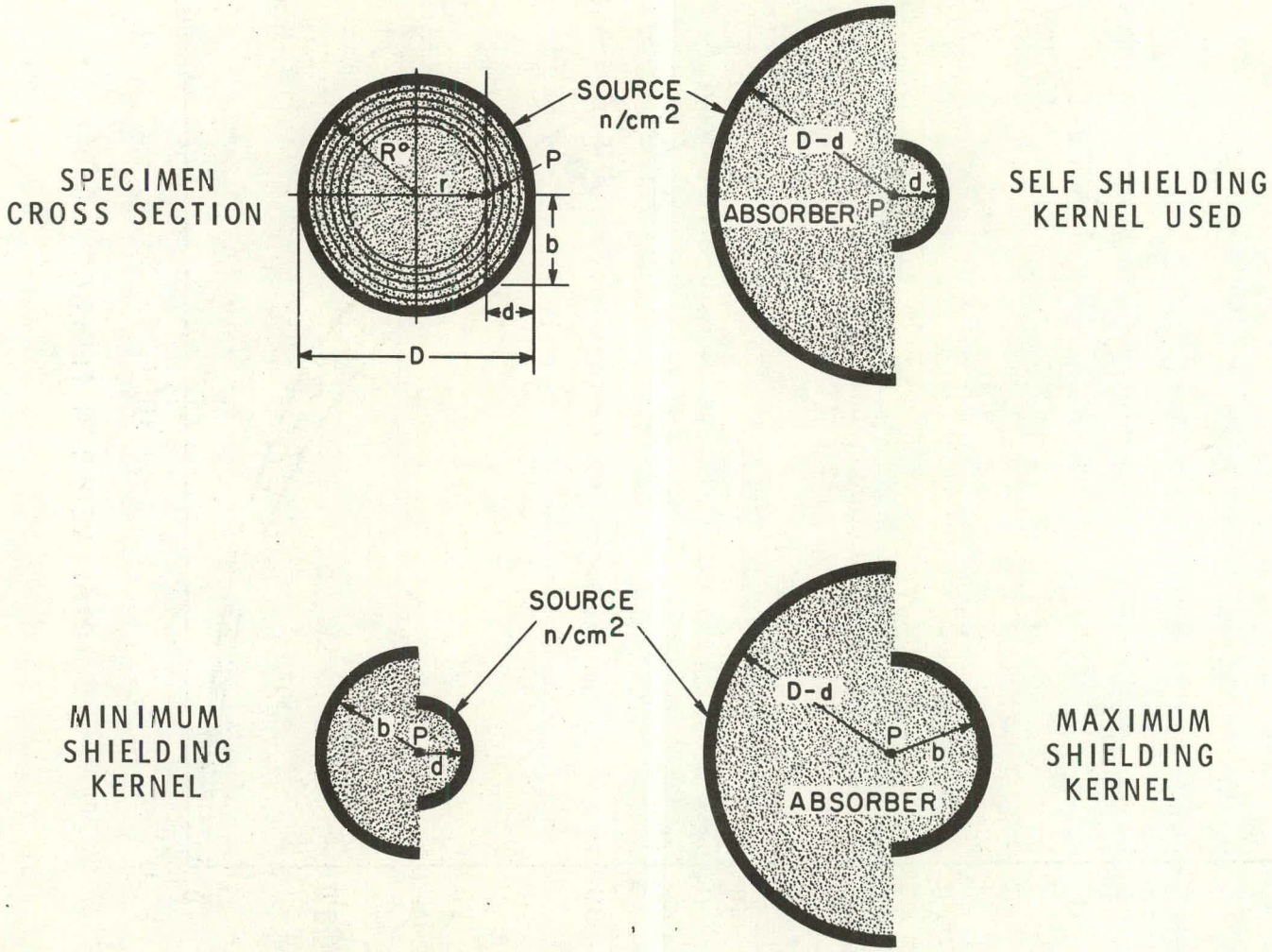

FIGURE 5. SOURCE AND SHIELDING KERNELS TO MODEL ABSORPTION AT POINT P

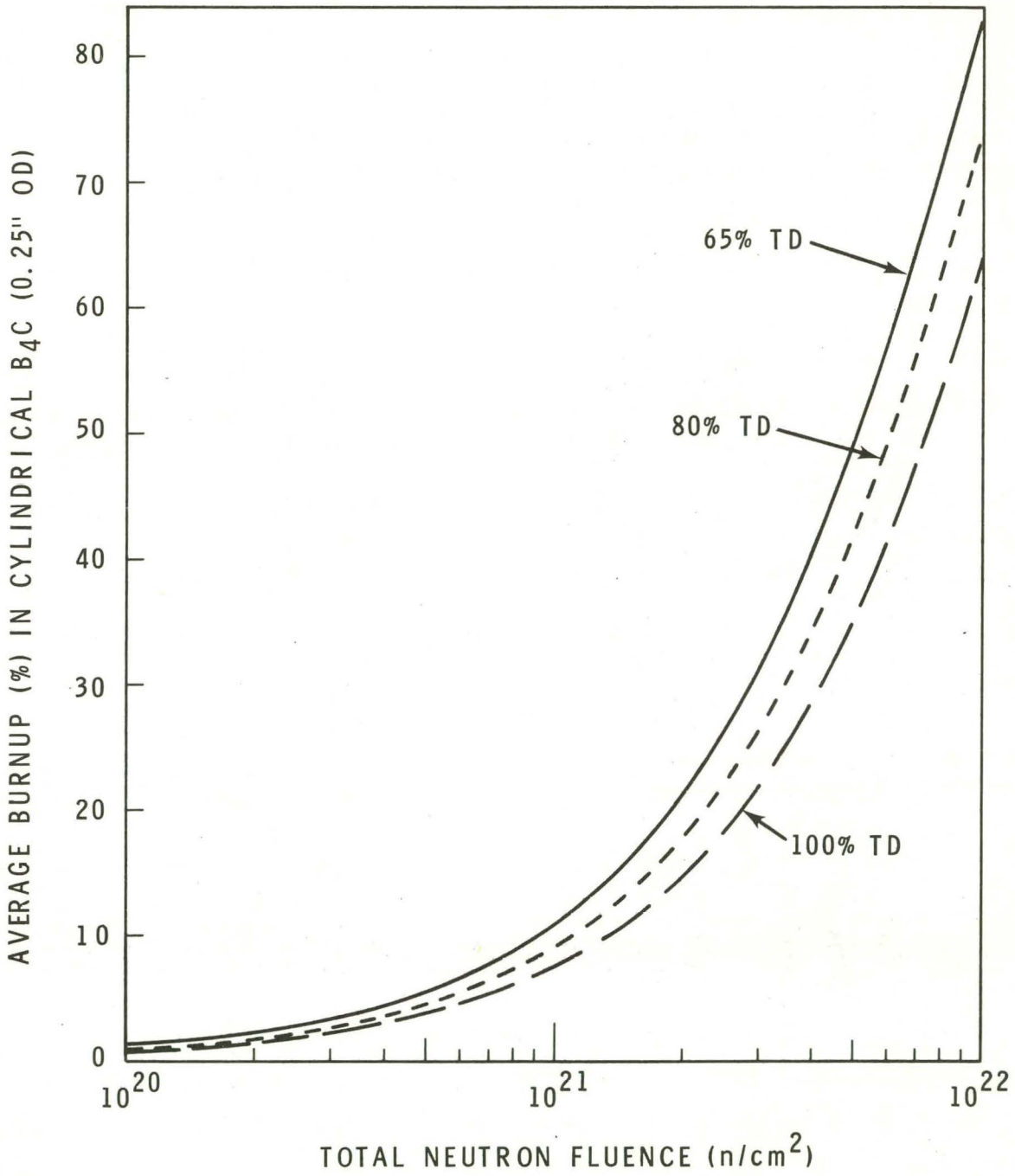

FIGURE 6. AVERAGE BURNUP IN B_4C CYLINDERS

TABLE III

AVERAGE ^{10}B BURNUP FOR
REPRESENTATIVE FLUENCES AND B_4C DENSITIES

Total Neutron Fluence $\Phi(n/cm^2)$	Density ρ(% TD)	Average Burnup $\overline{BU}$ (%)	Captures (cm^{-3})
$\Phi 1 = 1.0 \times 10^{22}$	100	$\overline{BU1} = 64$	4.4×10^{21}
	80	$= 74$	4.1×10^{21}
	65	$= 83$	3.7×10^{21}
$\Phi 2 = 1.65 \times 10^{21}$	100	$\overline{BU2} = 12$	8.4×10^{20}
	80	$= 15$	8.2×10^{20}
	65	$= 18$	7.9×10^{20}
$\Phi 3 = 9.5 \times 10^{20}$	100	$\overline{BU3} = 7.0$	4.8×10^{20}
	80	$= 8.6$	4.8×10^{20}
	65	$= 10.3$	4.6×10^{20}
$\Phi 4 = 4.5 \times 10^{20}$	100	$\overline{BU4} = 3.3$	2.3×10^{20}
	80	$= 4.1$	2.3×10^{20}
	65	$= 4.9$	2.2×10^{20}

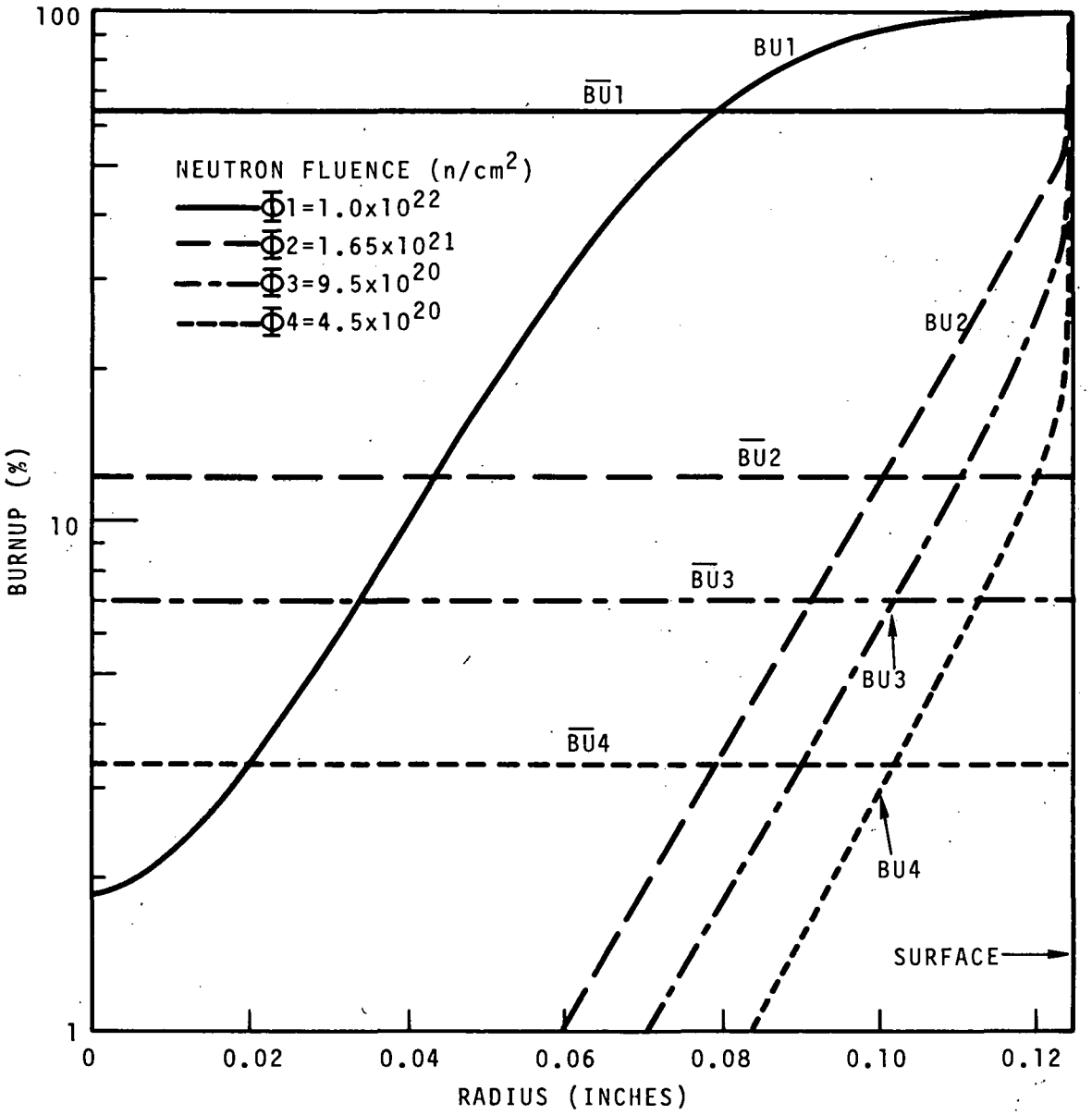

FIGURE 7. LOCAL (BU) AND AVERAGE ($\overline{BU}$) ^{10}B BURNUP IN 0.250 INCH OD CYLINDERS OF 100% TD B_4C

calculated for subassemblies 3, 5, and 6. Table IV shows the measured burnup, calculated burnup, and the calculated fluence for representative specimens of each subassembly. Mass spectroscopic analysis of the powdered specimen burnup data (also shown in Table IV) were also used to verify the analytical approach for calculating the ^{10}B burnup in pellet and powdered samples.

TABLE IV

CALCULATED ^{10}B BURNUP AND

TOTAL FLUENCES FOR B_4C CYLINDERS IN THE K REACTOR

Density (% TD)	Measured ^{10}B Burnup (%)	Calculated ^{10}B Burnup (%)	Calculated Captures (cm^{-3})	Calculated Fluence (n/cm^2)
Subassembly 1				
100		3.50	7.60×10^{20}	4.70×10^{20}
80	4.12	4.09	7.14×10^{20}	4.50×10^{20}
65	5.27	5.28	7.49×10^{20}	4.85×10^{20}
Subassembly 2				
100		9.56	2.09×10^{21}	1.30×10^{21}
80	11.04	11.3	1.97×10^{21}	1.25×10^{21}
65	14.95	15.0	2.13×10^{21}	1.40×10^{21}
Subassembly 3				
100		12.1	2.64×10^{21}	1.65×10^{21}
80		14.8	2.58×10^{21}	1.65×10^{21}
65		17.6	2.50×10^{21}	1.65×10^{21}
Subassembly 4				
100		7.00	1.53×10^{20}	9.50×10^{20}
80	8.55	8.59	1.50×10^{20}	9.50×10^{20}
65	10.30	10.3	1.46×10^{20}	9.50×10^{20}
Subassemblies 5 and 6				
100		11.7	2.56×10^{21}	1.60×10^{21}
80		14.4	2.51×10^{21}	1.60×10^{21}
65		17.1	2.43×10^{21}	1.60×10^{21}

Helium production as a function of fluence was also calculated for the specimens. The results are shown in Figure 8. The gas volume produced is determined by the number of ^{10}B atoms transmuted. For example, at a fluence of 10^{21} n/cm^2 average burnup is 7.6% in 100% TD material, but 10.9% in 65% TD material. However, Figure 8 shows approximately equal helium production for these specimens. At higher fluences, the theoretical helium production is higher for the fully dense material than for the 65% TD material.

Irradiation data were obtained for an average burnup range of 3.5-18% ($\sim$7, 21, and 26 x 10^{20} captures/cm^2) in the 600° - 1200°F test and for a burnup range of 7-17% ($\sim$15 and 25 x 10^{20} captures/cm^3) in the 500 - 700°F assembly.

RESULTS

Gas Release

The results of the gas release measurements for the various sample forms are shown in Figures 9 through 12. The data from all five exposure levels are plotted on a single figure for each material type. There appears to be no consistent correlation between fluence and gas release fraction, and one curve was drawn through all the data for each sample form. The reader is referenced to Figure 7 and Table IV to obtain actual burnup profiles and reaction levels in the samples as a function of exposure.

The powder samples (Figure 9) show the highest gas release fraction. The percent helium release increases from $\sim$10% at 500°F to about 30% at at 850°F. There is no apparent difference in gas release behavior between the loose-packed and vibrationally-compacted materials. The 65 and 85% TD pellets (Figures 10 and 11) display generally similar gas-release behavior. They retain more of the gas than do the powders, releasing $\sim$6-8% of the helium at 500°F and $\sim$25% at 1100°F. The similarity in the gas release behavior of the 65 and 80% TD pellets might be expected from observations made of the microstructure of the materials (Figures 2 and 3). Both pellet types were fabricated from similar coarse-grain feed stock, and the porosity of both pellet types is essentially open. Consequently, once the helium has escaped the grains, it has essentially free access to the capsule plenum. The gas release fraction in the 99% TD pellets (Figure 12) is significantly less than for any of the

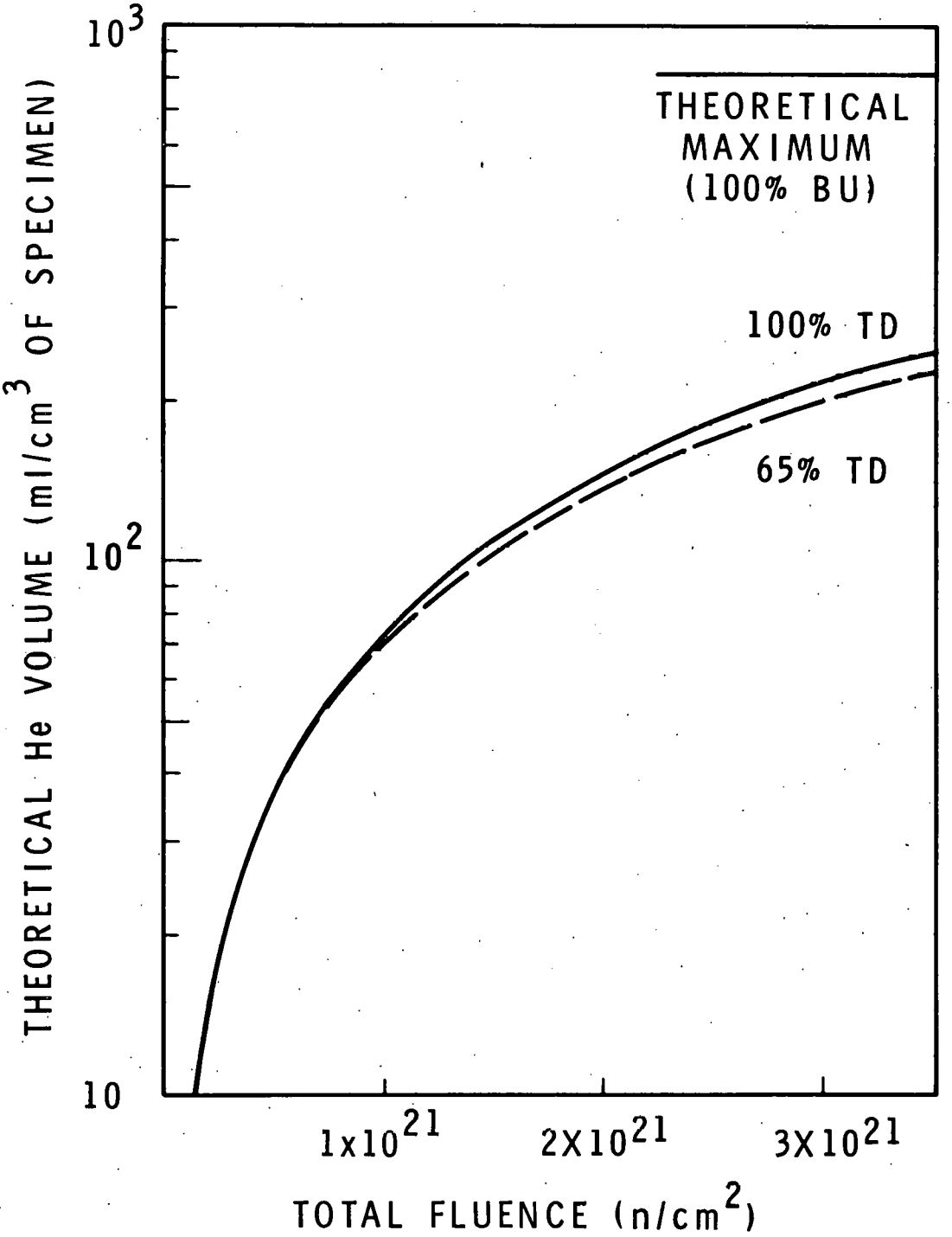

FIGURE 8. THEORETICAL He PRODUCTION AT STP

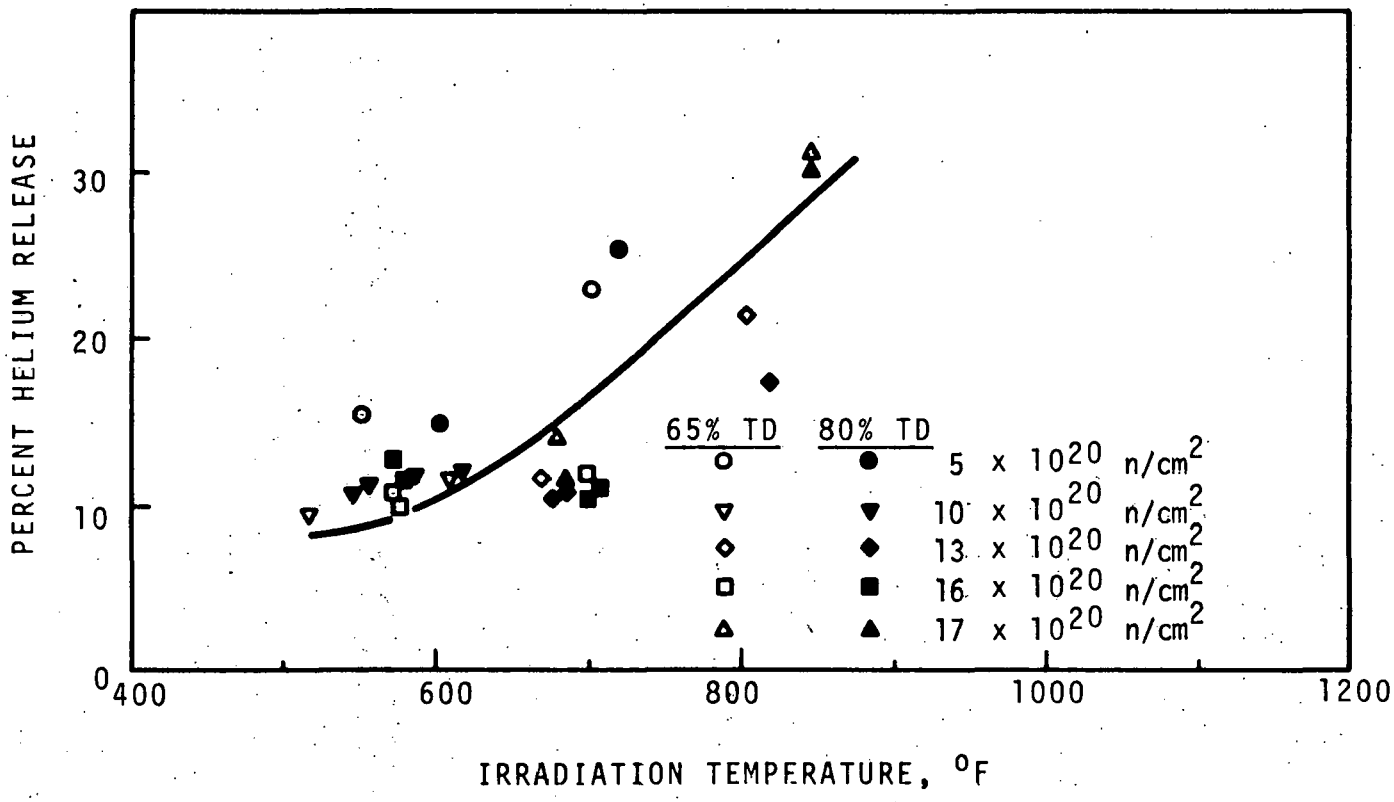

FIGURE 9. GAS RELEASE BEHAVIOR OF B_4C POWDERS

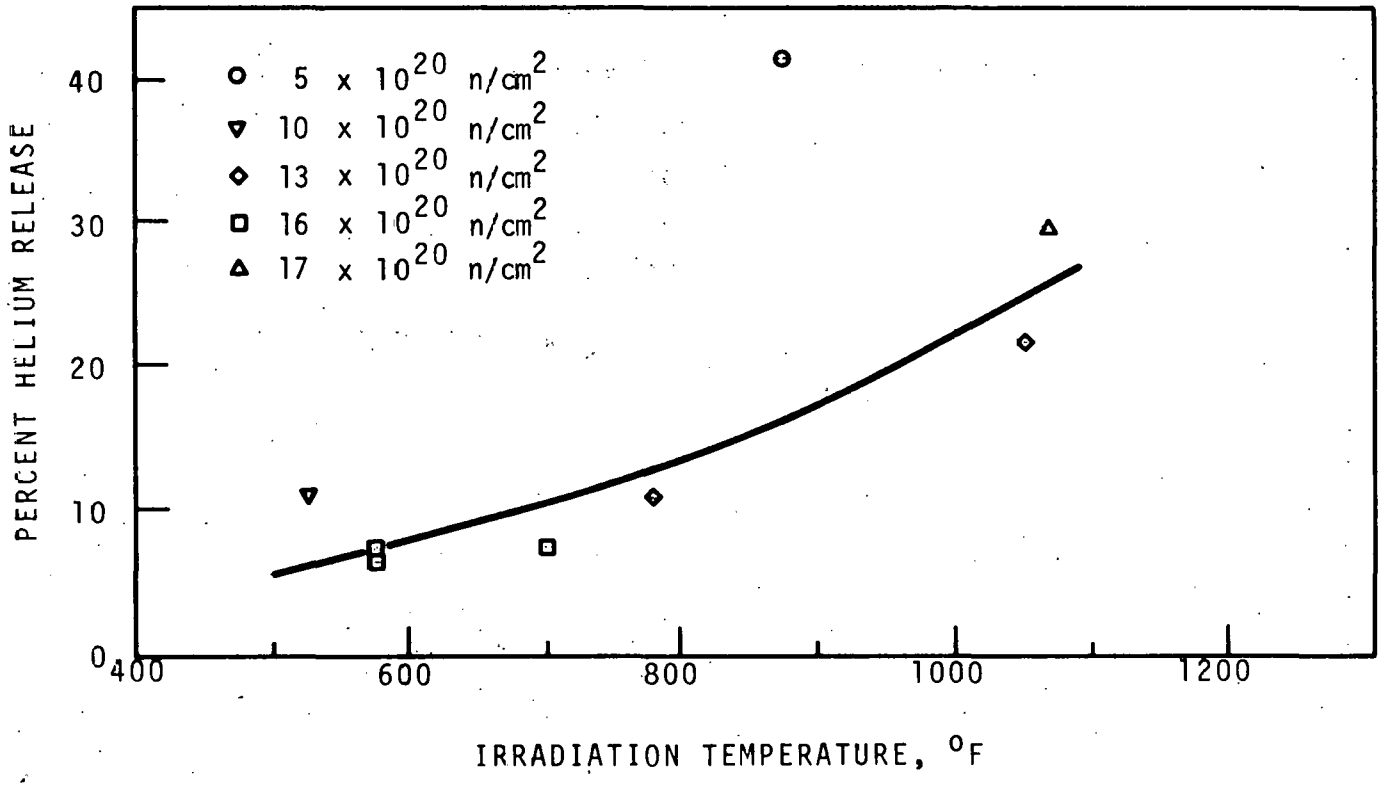

FIGURE 10. GAS RELEASE BEHAVIOR OF 65% TD PELLETS

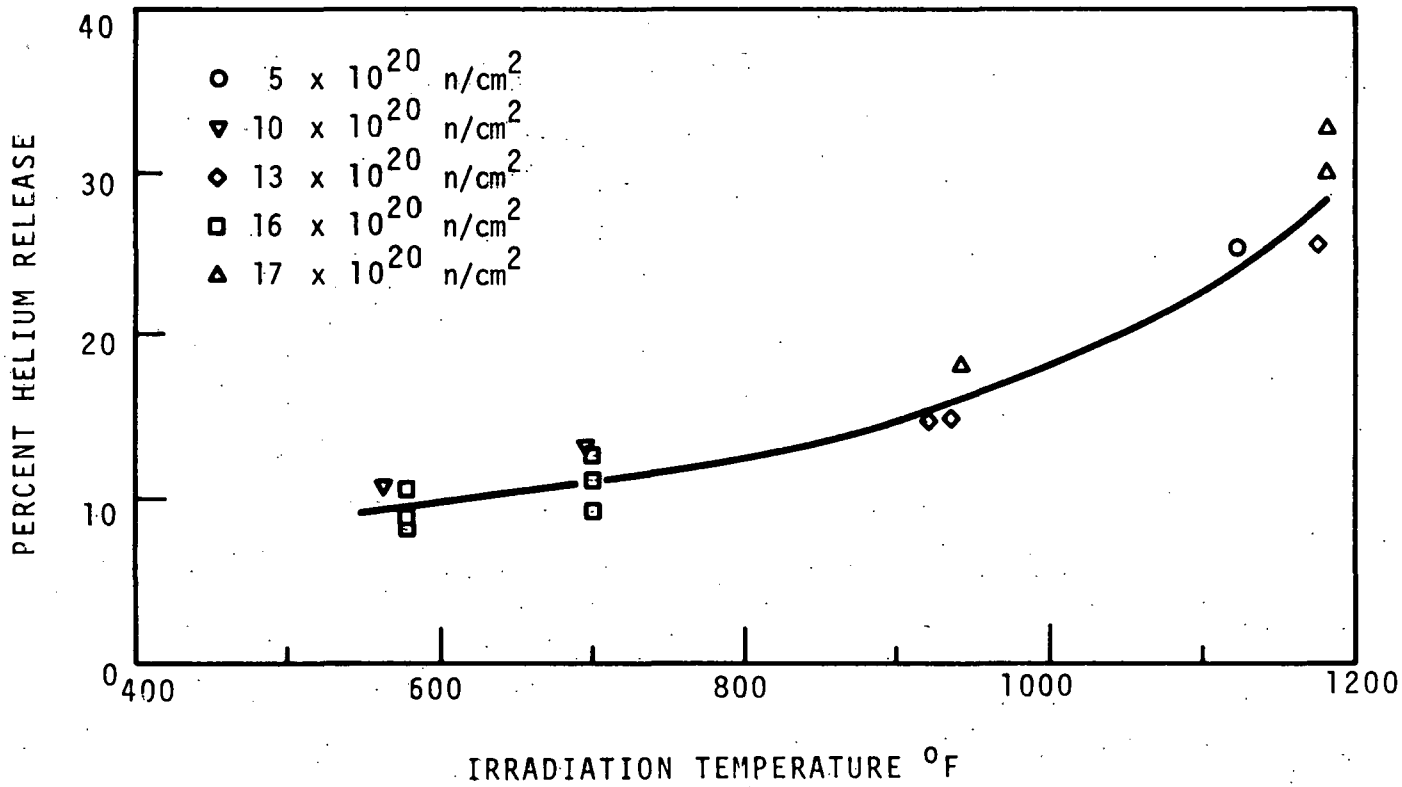

FIGURE 11. GAS RELEASE BEHAVIOR OF 80% TD PELLETS

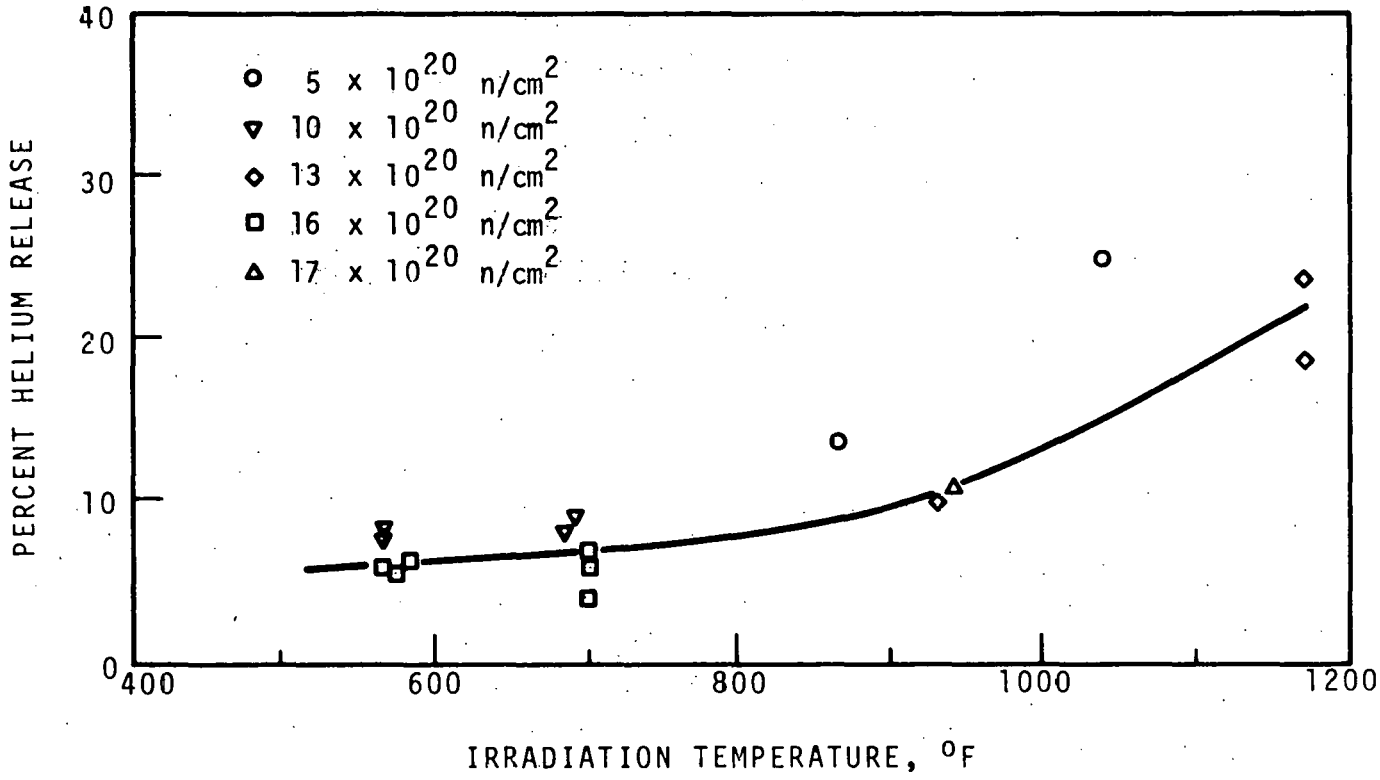

FIGURE 12. GAS RELEASE BEHAVIOR OF 99% TD PELLETS

other materials. Approximately 5% of the helium is released at 500°F, increasing to ~20% at 1200°F. The temperature dependence of the gas release fraction is very evident in all forms of the B_4C. In the pellets, the amount of gas released appears to increase rapidly as the irradiation temperature exceeds 1000°F.

Figure 13 shows the effect of pellet density on gas release over a broad density range. The apparent lower release fraction in the 65% TD at temperatures below 800°F is probably due to experimental scatter. As indicated above, the microstructure of the 65 and 80% TD pellets would suggest little difference in gas-release behavior. However if any differences were evidenced, they would be expected to be in the direction of less gas release for the 80% TD pellets because of a lower total surface area in these specimens. Gas release is seen to decrease significantly as theoretical density is approached. Although the curves have been drawn to indicate a gradual reduction in gas release as the pellet density increases, in reality this may not be the case. It might be expected that the gas release fraction would be relatively independent of pellet density until near-theoretical densities were attained, at which point the release fraction would decrease rapidly. Present fabrication techniques often are prone to producing pellets with significant density variations on the high density end of the spectrum (90-99% TD). Consequently a study to accurately determine the irradiation behavior of B_4C pellets as a function of density in the 90-99% TD range would appear warranted.

Swelling

Visual examination of the samples during capsule disassembly showed that the pellets suffered considerable degradation as a result of the irradiation. Corners were rounded, cracks were prominent, and the pellets were mostly broken into smaller particles. The surfaces of many pellets were delaminated and flaky, particularly so in the 99% TD pellets. All the powders and pellets were stuck in their holders and had to be forced out. A 0.010 inch diametrical gap had been allowed between the 0.25 inch diameter pellets and their holders. Again, the 99% TD pellets were the most difficult to remove. This apparent greater swelling tendency in

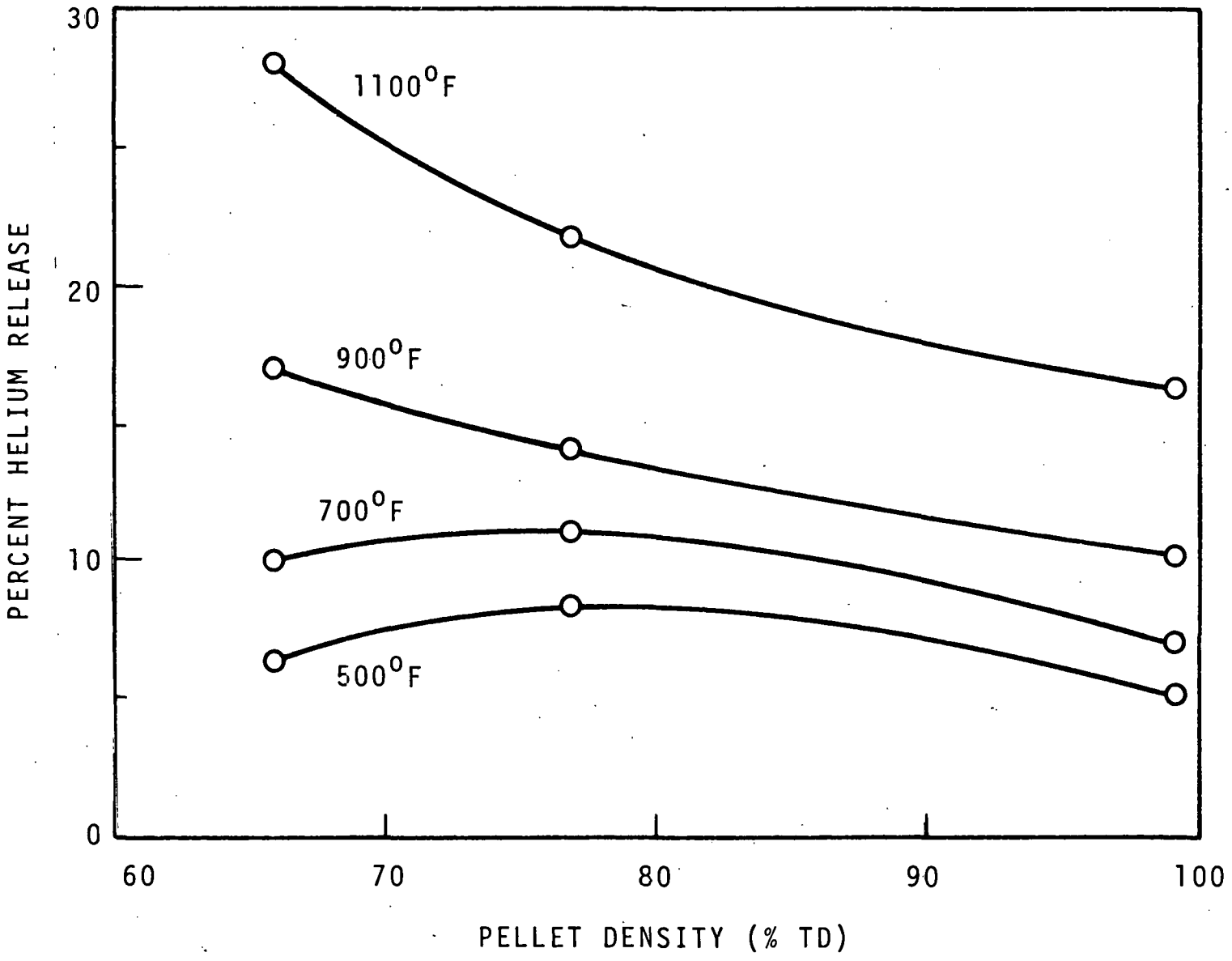

FIGURE 13. GAS RELEASE AS A FUNCTION OF PELLET DENSITY

the 99% TD pellets is consistent with the lower gas release fraction seen in this material. An attempt to measure pellet densities after irradiation by immersion weighing in water proved unsuccessful. Values obtained by this method were always near theoretical density, indicating that the porosity and cracks generated during irradiation were accessible to the water.

Microstructure

Several specimens were selected for metallographic examination after irradiation. Figure 14 shows the microstructure of a 99% TD pellet that was irradiated to 3.5% ^{10}B burnup (7.6×10^{20} captures/cm^3) at 865°F. The micrograph is compared with a calculated burnup distribution, illustrating that the internal region of the sample where microstructure appears undergraded, has suffered very little ^{10}B burnup. The exterior of this high density pellet has experienced ^{10}B burnup many times more severe than the average pellet burnup $\overline{BU}$. However, because of the destructive surface fragmentation, delamination, and extensive swelling in this region, it would be misleading to attach an absolute calculated ^{10}B burnup value to the boundary of surface delamination, without substantiating experimental evidence.

This classic illustration of "skin burnup" in high density B_4C depicts swelling, circumferential cracking, and considerable particle separation in in the cracked area. In contrast, the core of the pellet appears unaffected by the irradiation. The lower density pellets, however, do not display this skin effect. Figure 15 shows the microstructure of a 80% TD pellet irradiated to 4% ^{10}B burnup at 1120°F. Here, radial cracking is present throughout the pellet. There is no apparent difference in the microstructure between surface and core regions. The 65% TD pellets have a similar metallographic appearance. The contrast in the behavior of the high- and low-density pellets may be a result of the difference in strength and ductility in the materials. As the surface of the high-density pellet experiences severe irradiation damage, it swells and breaks away from the stronger, unreacted core. In the lower-density pellets, however, the greater ductility may accommodate the surface swelling more readily without the severe deterioration seen in the 99% TD pellets. Also, stresses generated from surface swelling are transmitted to the core and cause cracking in the lower-strength material.

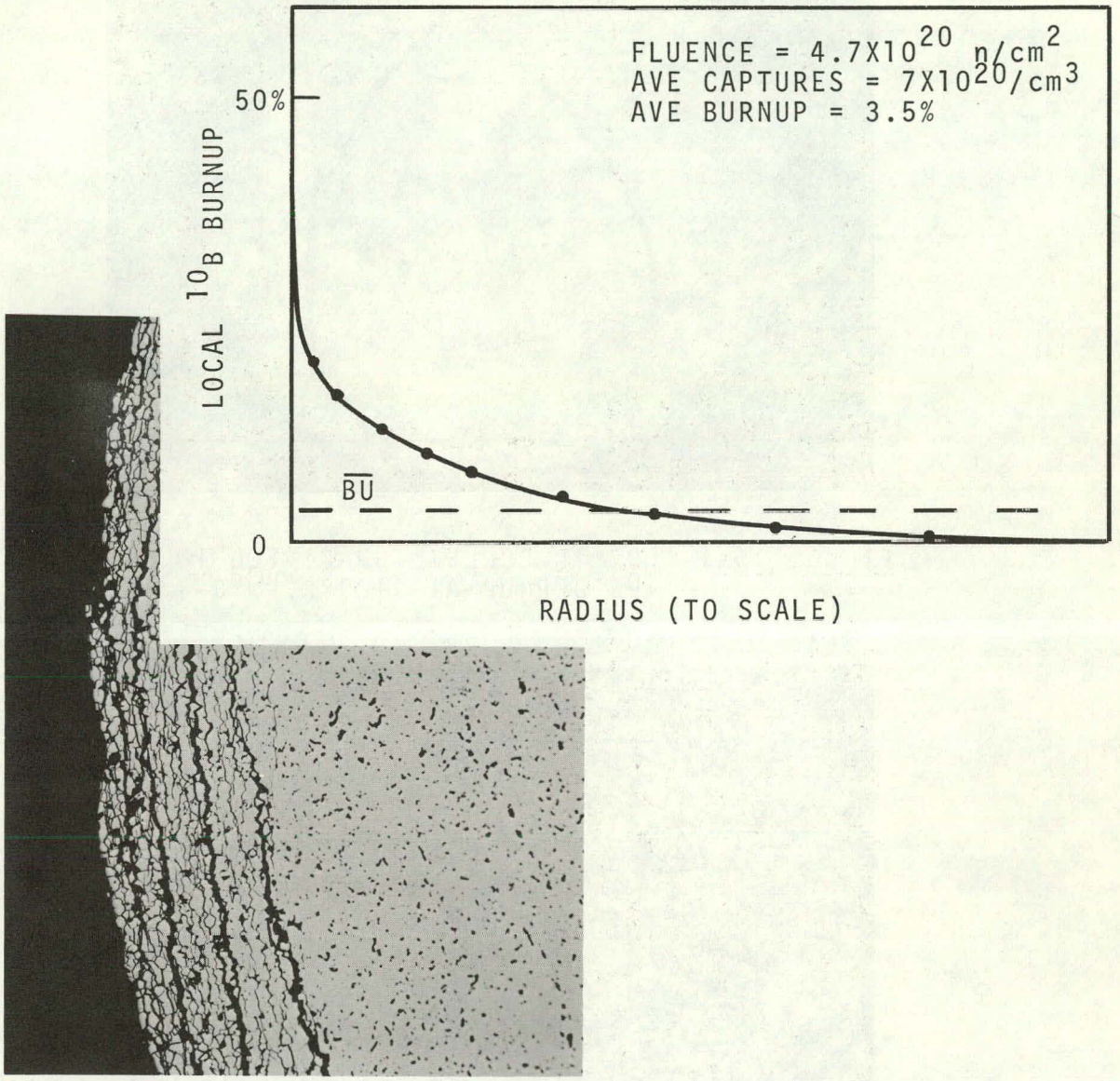

FIGURE 14. 99% TD PELLET IRRADIATED TO ~3.5% ^{10}B BURNUP AT 865°F (80X), COMPARED WITH AN ILLUSTRATIVE BURNUP DISTRIBUTION

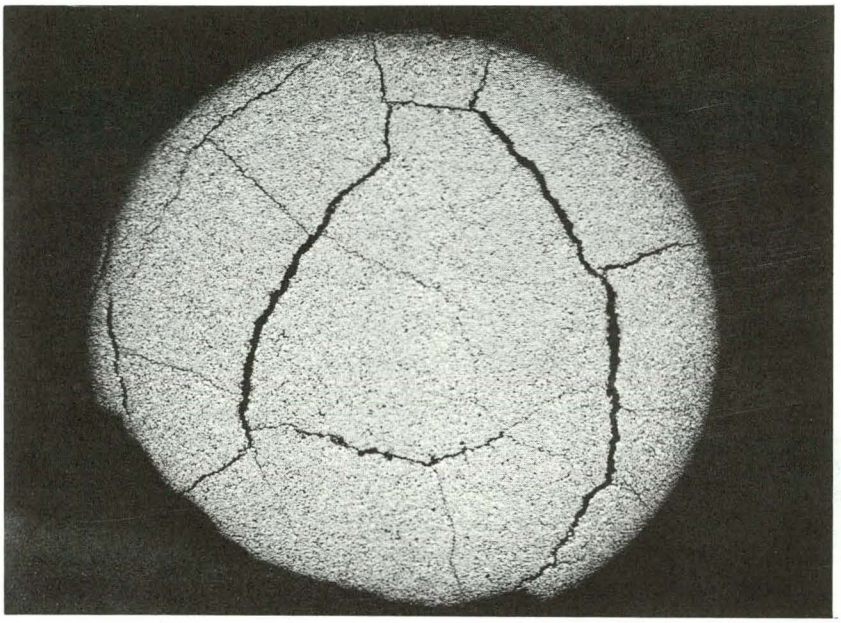

FIGURE 15a. 80% TD PELLET IRRADIATED TO ~4% ^{10}B BURNUP AT 1120°F. 13-1/2X

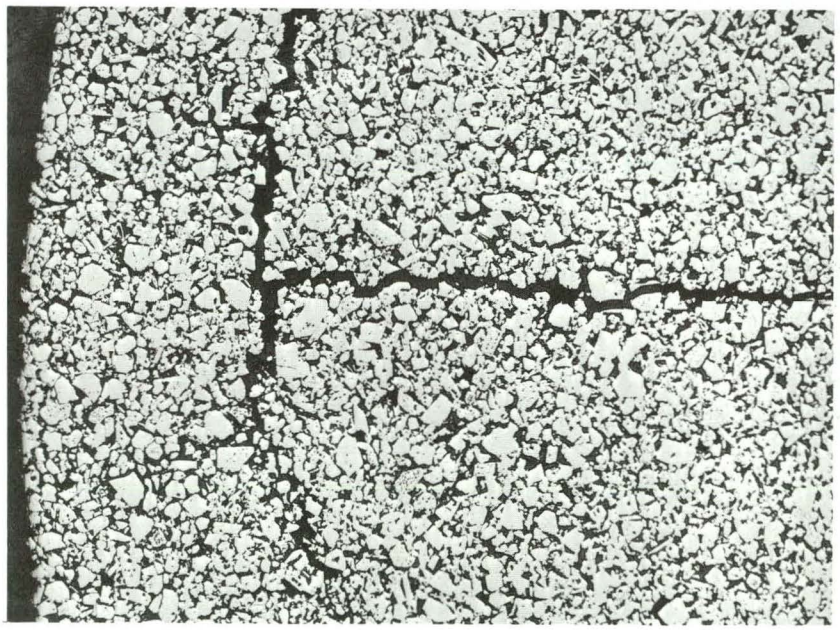

FIGURE 15b. 80% TD PELLET IRRADIATED TO ~4% ^{10}B BURNUP AT 1120°F. 80X

Some pellets irradiated to ∿9% ^{10}B burnup (∿15 x 10^{20} captures/cc) were also examined metallographically. The lower-density pellets had appearances similar to those of pellets irradiated to 4% ^{10}B burnup. The 99% TD pellets, however, had a markedly different appearance at the higher exposure. Figure 16 shows the microstructure of a 99% TD pellet irradiated to 9% ^{10}B burnup at 565°F. The peripheral damage is still apparent, with the outer shell of the pellet completely detached from the inner core. Circumferential cracking and particle separation are again common in the shell portion. However, the core of the pellet also shows damage at this exposure. There is uniform cracking in the material all the way to the center of the pellet, and the cracks often seem to penetrate into grains. It is possible that at this higher exposure, the damage contributed by fast neutrons (which would be uniform throughout the material) is great enough to cause the observed effects.

While very little damage could be detected in powder particles irradiated to ∿4% ^{10}B burnup, particles irradiated to ∿9% ^{10}B burnup did show effects of the irradiation when examined metallographically. Figure 17 shows the cracking that occurred in a -10 +20 mesh particle that was probably near the surface and consequently experienced high burnup. Other particles examined did not show such a severe state of damage. A very unusual example of particle cracking is shown in Figure 18. This B_4C particle was also -10 +20 mesh and was irradiated to ∿9% average ^{10}B burnup. The particle contains second phase graphite, identified as the darker areas in the micrograph. The irradiation has caused the adjacent B_4C to curl into the graphite, presumably because of a lack of restraint in the graphite regions. The amount of deformation is quite surprising.

Transmission optical microscopy was used in an attempt to locate clustered products from the $^{10}B(n,\alpha)^7Li$ reaction in irradiated B_4C. A 99% TD pellet irradiated to ∿4% ^{10}B burnup at 875°F was thinned mechanically by hand polishing on diamond grinding wheels and then was polished in a diamond slurry. A micrograph of the sample is shown in Figure 19. The grain boundaries of the irradiated material contain objects assumed to be clustered lithium and/or helium voids. The grain boundaries of an unirradiated specimen examined in this manner were free from these concentrations.

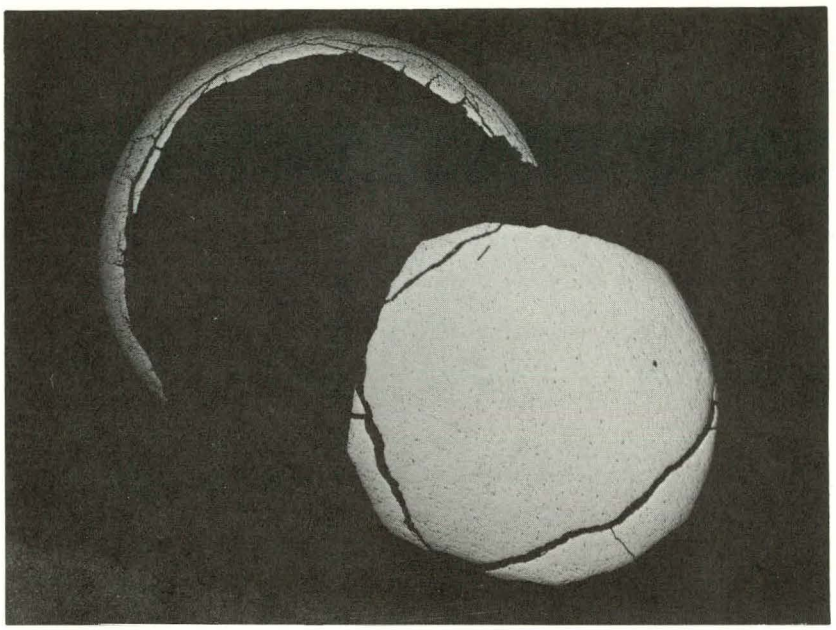

FIGURE 16a. 99% TD PELLET IRRADIATED TO ~9% ^{10}B BURNUP AT 565°F. PELLET AND DETACHED SHELL. 9X

FIGURE 16b. 99% TD PELLET IRRADIATED TO ~9% ^{10}B BURNUP AT 565°F. SHELL REGION. 160X

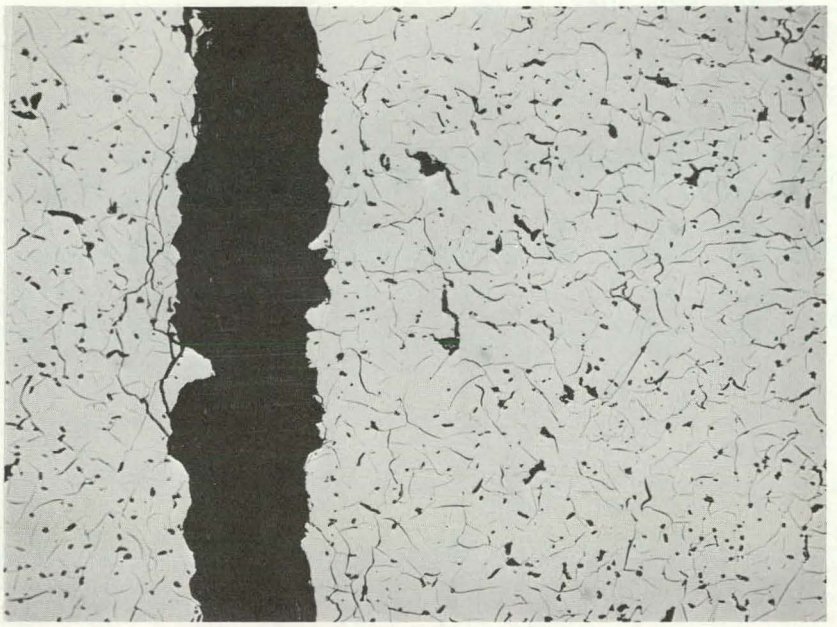

FIGURE 16c. 99% TD PELLET IRRADIATED TO ~9% ^{10}B BURNUP AT 565°F. CORE REGION. 160X

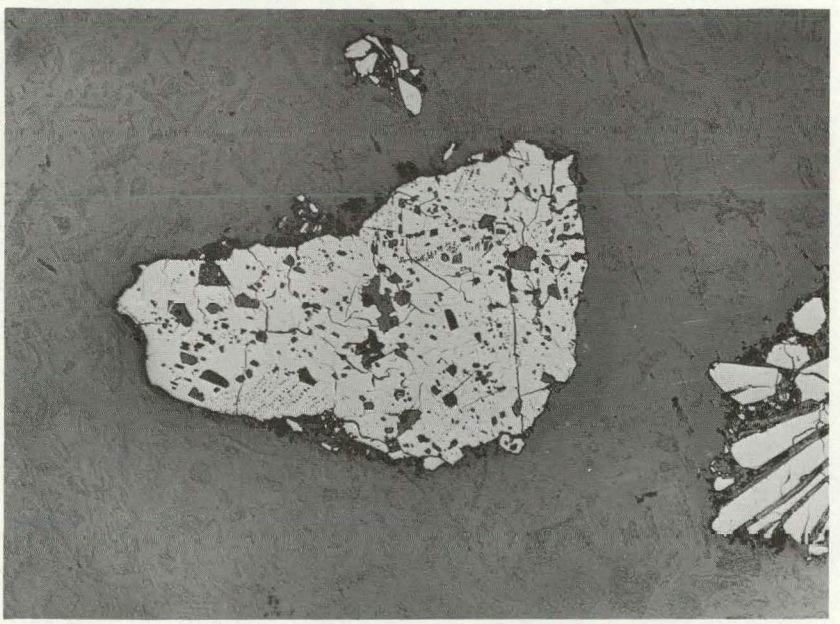

FIGURE 17. CRACKING IN B_4C PARTICLE IRRADIATED TO ~9% ^{10}B BURNUP AT 550°F. 100X

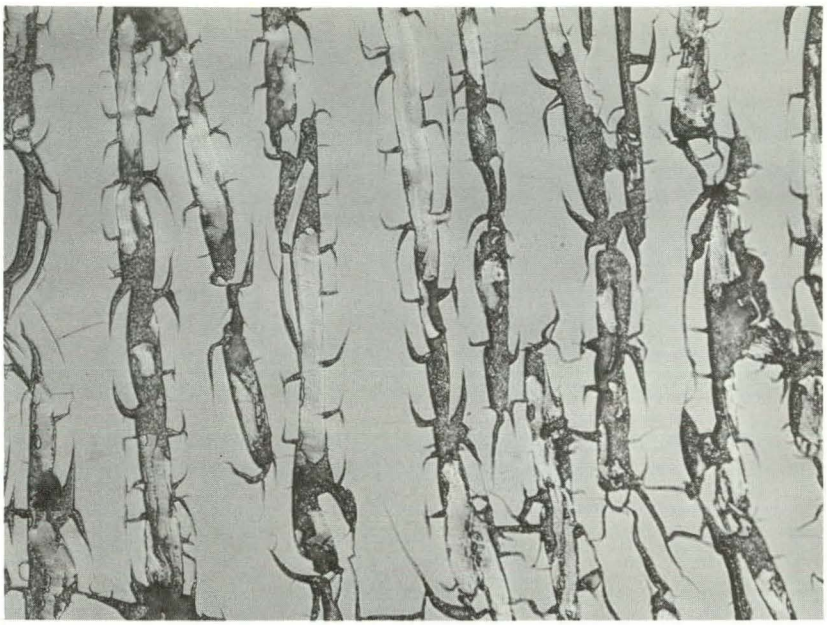

FIGURE 18. B_4C PARTICLE IRRADIATED TO ~9% BURNUP AT 550°F. SHOWING CURLING OF B_4C INTO ADJACENT GRAPHITE REGIONS. 400X

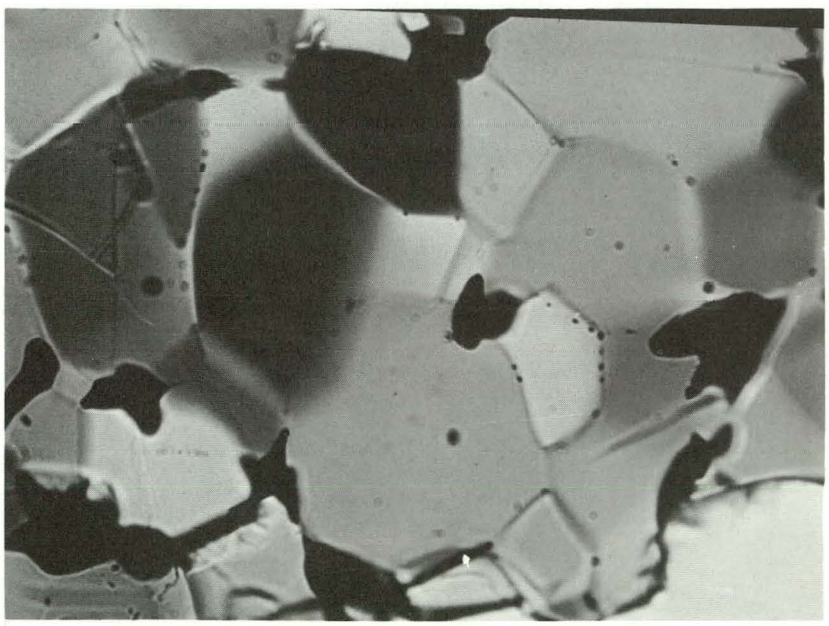

FIGURE 19. TRANSMISSION OPTICAL MICROGRAPH OF 99% TD PELLET IRRADIATED TO ~4% ^{10}B BURNUP AT 875°F. DARK OBJECTS ALONG GRAIN BOUNDARIES ARE $^{10}B(n,\alpha)^{7}Li$ REACTION PRODUCTS. 1240X

B_4C - Cladding Interaction

Metallography was performed on a 99% TD pellet in its 304 stainless steel holder after irradiation to ~12% ^{10}B burnup (21 x 10^{20} captures/cc) at 1170°F. No indication of interaction between the materials could be detected.

A test was performed to determine whether irradiated B_4C might be inferior to unirradiated material with respect to compatibility with 316 stainless steel. Scraping from an irradiated pellet (which would have experienced very high burnup) were placed in 316 stainless steel holders and heated for 1000 hours at 1025 and 1110°F. Samples of unirradiated -325 mesh B_4C powder were placed in identical holders as standards. The results were identical; neither of the specimens at 1025°F reacted with their holder, but both samples at 1110°F formed a 2.5 micron reaction layer with the stainless steel. Therefore it appears that irradiation of B_4C does not reduce its compatibility with 316 stainless steel.

X-Ray Diffraction

Scrapings taken from the surface of irradiated pellets were examined by x-ray diffraction, but the results were very scattered. These surface scrapings presumably experienced very high burnup. Gray and Lyman (2) have previously studied the effect of irradiation on the lattice parameters of B_4C and reported that at high burnup the a_o value remained unchanged while the c_o parameter decreased 2.9%. In the present examination, the c_o lattice parameter was found to have decreased in general from 2 to 4%. No lithium compounds, such as the carbide or boride found by Secreist (9) in out of reactor tests, could be detected in the irradiated material by x-ray diffraction.

Sodium Compatibility

A 99% TD pellet irradiated to 4% ^{10}B burnup at 1130°F was exposed to sodium at 940°F for 1000 hours. The pellet broke into several smaller pieces during the test. The metallographic appearance of the exposed

material is shown in Figure 20. There is uniform cracking to the center of the pellet. As indicated previously (Figure 14), the core of this material showed no effect from the irradiation prior to the sodium exposure. An unirradiated 99% TD pellet exposed to sodium under similar conditions showed negligible weight loss. Some edge cracking was exhibited, but it is suspected that this was a result of fabrication stresses. Similar pellets that were heated to 2000°C and cooled slowly prior to exposure to sodium were essentially free from cracks after 1000 hours in sodium at 940°F.

An 80% TD pellet irradiated to ~4% ^{10}B burnup showed similar microcracking throughout its core after exposure to sodium. It appears that if stresses are present in B_4C pellets, exposure to heated sodium will cause development of a crack structure that was previously undetectable. Therefore it would seem conceivable that this technique could be used to examine B_4C pellets for internal stresses.

DISCUSSION

The large thermal-neutron absorption cross section of ^{10}B is known to cause considerable self shielding within B_4C absorber in thermal reactor irradiation. Consequently it might be expected that sample geometry could have a large influence on the irradiation behavior of boron carbide. Another consideration that must be recognized in thermal reactor testing of B_4C is that while the thermal portions of the spectra are basically similar for the various reactors, epithermal and high-energy portions of the spectra can vary significantly between different facilities. Therefore damage in B_4C resulting from interactions with higher-energy neutrons could conceivably result in different overall performance of B_4C in various reactors under similar temperature and burnup conditions. In recognition of these potential problems in interpreting thermal reactor data, analytical calculations were performed in conjunction with this experiment to give some definition to possible effects of geometry and various thermal reactor spectra on the irradiation behavior of boron carbide.

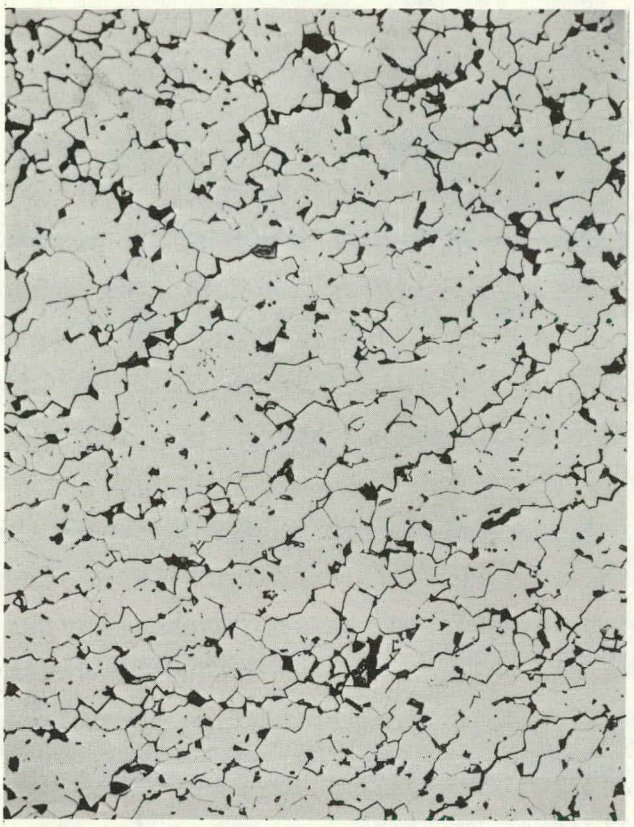

FIGURE 20. 99% TD PELLET IRRADIATED TO ~4% ^{10}B BURNUP AT 1130°F EXPOSED TO SODIUM AT 940°F FOR 1000 HOURS. CRACKS WERE ABSENT PRIOR TO SODIUM EXPOSURE.

Specimen shapes in irradiation testing of B_4C have generally been chosen as cylinders and discs or slabs. Therefore these two geometries were selected for the comparative calculational analysis. The computational techniques described earlier to calculate reaction densities for the K Reactor cylindrical samples were also adapted to planar slab geometry. ^{10}B atom densities were calculated as a function of depth and fluence, and the results are shown in Figure 21. It is seen that burnup near the surface of the slab is higher than near the surface of the cylinder. As expected, when the radius of the cylinder increases, the distribution for the cylinder approaches the distribution for the slab. The average burnup of a slab specimen and of a cylinder specimen of equal thickness could differ by approximately 50% in the K Reactor irradiations at a fluence of 10^{21} n/cm^2. Thus, assuming that both achieved the same average burnup would lead to a 50% error in their comparable gas volume production estimates. A slab or disc of boron carbide exhibits greater surface burnup than a comparable cylindrical specimen, independent of material density and fluence.

Three typical thermal reactors were chosen for the spectral effects analysis; K, ETR, and NRU. For these computations a set of nineteen group-averaged n,α capture and neutron transport cross sections were used. These nineteen group cross sections were used with the core region neutron spectrum to calculate a unique spectrum-averaged cross section ($\overline{\sigma}$) for each reactor. The differences in low energy neutron spectra among the reactors are reflected in the $\overline{\sigma}$ $^{10}B(n,\alpha)$ cross sections in Table V. The $\overline{\sigma}$ for K is nearly 63% greater than for ETR, while $\overline{\sigma}$ for K and NRU varies by only 4%. These results show that irradiation to equal fluence in these three reactors can lead to substantially different helium production partly because of the difference in the reactor core spectra. The difference in helium production would be even more pronounced at out-of-core locations.

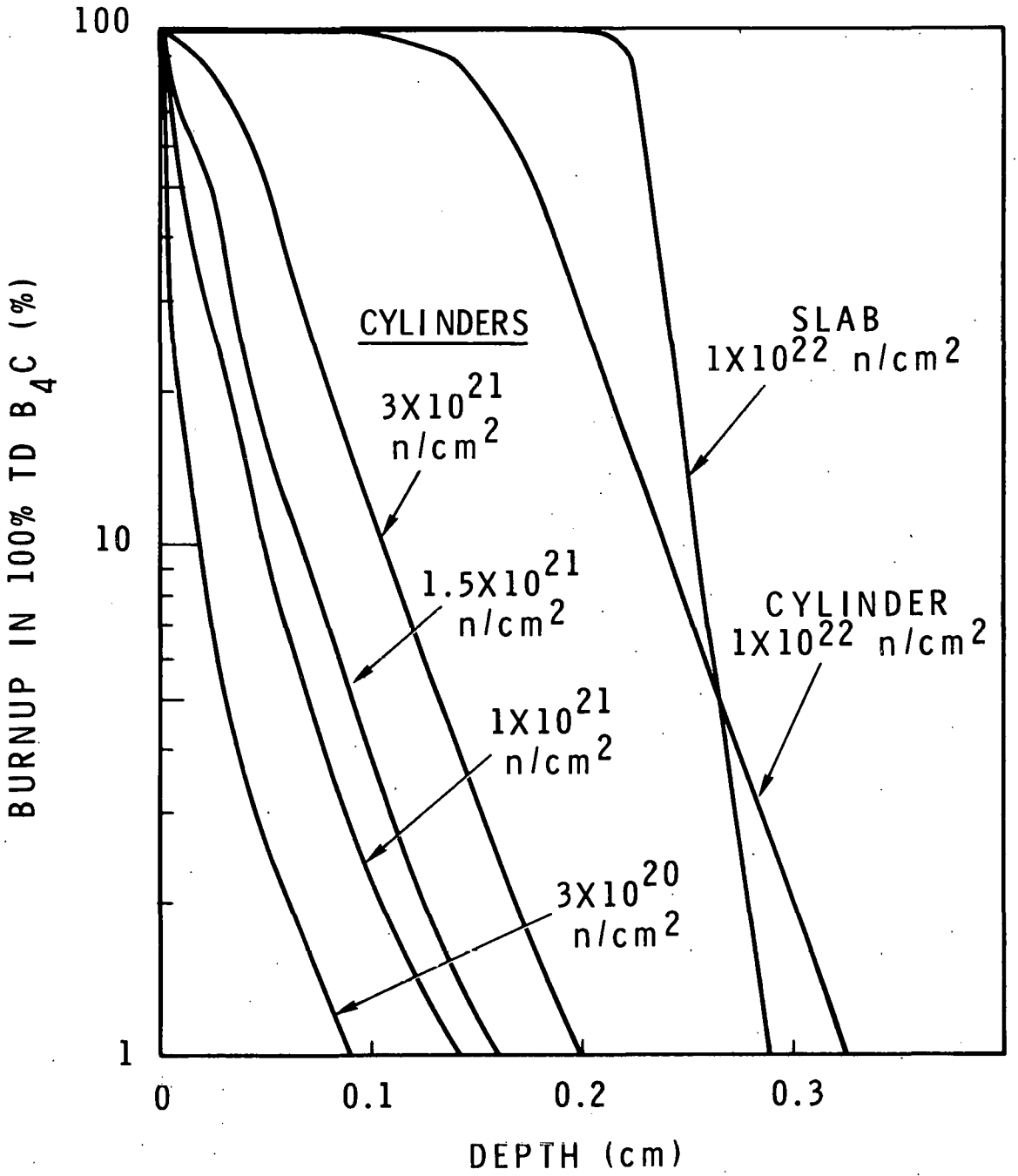

FIGURE 21. LOCAL BURNUP DISTRIBUTIONS

TABLE V

IRRADIATION DAMAGE TO B_4C IN THERMAL REACTORS

Reactor	$\bar{\sigma}_{10B(n,\alpha)}$ (barns)	(n,α) Displacements / (n,n) Displacements	Other Reactor (n,n) / K Reactor (n,n)
K	1006	670	1.0
ETR	619	383	1.01
NRU	965	531	1.22

This spectral dependence also is found in displacement production. Two processes can cause displacements. One, the recoil lithium and alpha particles from the n,α capture process have sufficient energy to displace atoms from the lattice structure. Evaluations for boronated graphite led to the result of 1400 displacements per n,α interaction (10, 11). The second mechanism for displacement production is neutron scattering. Energetic knock-on atoms of the lattice dissipate their energy by causing additional displacements. The number of displacements from each neutron scattering incident depends on the energy of the neutron (12). Displacement production from these mechansims have also been evaluated for K, NRU, and ETR. These evaluations permit a comparison of relative displacement production as a function of fluence and the relative importance of the two damage mechanisms.

Table V gives the ratio of displacements caused by n,α capture to the displacements caused by neutron scattering at the surface of a B_4C specimen. Although the displacements caused by n,α reactions are the dominant damage mechanism near the B_4C surface in all three reactors, it must be remembered that the n,α reactions decrease drastically with depth into the specimen while neutron scattering displacement damage remains nearly constant through the material. Consequently, a good percentage of the damage within the B_4C can be caused by fast neutron scattering. Table V also compares the scattering displacement production per unit fluence among the three reactors. While the K and NRU reactors are quite comparable in theoretical helium production and (n,α) displacement production, the ETR is nearly identical to the K in producing fast neutron scattering damage. It can be seen how

different damage accumulation can result from equal exposures in different reactors.

Figure 22 shows the energy range of neutrons which cause 90% of each damage mechanism in the three reactors. In ETR, more neutrons of epithermal energy are involved in many of the n,α reactions as compared to the situation in NRU or K. Since epithermal neutrons are attenuated less than thermal neutrons in B_4C, the damage distribution in a specimen irradiated to a given fluence in ETR would be significantly different from that of a specimen irradiated in NRU or K to an equal fluence. The response range for scattering displacement damage is quite comparable among the three reactors. However, different ratios of fast to thermal fluence for these reactors dictate different high energy neutron damage for specimens irradiated to equal total fluence or even to equal ^{10}B burnup, in these reactors. These differences could easily result in dissimilar irradiation performance of the B_4C.

CONCLUSIONS

Boron carbide irradiated in Hanford thermal production reactors at 500-1200°F to a maximum average ^{10}B burnup of 18% showed a definite dependence of gas release on specimen form and irradiation temperature. Powder samples of comparable densities released more gas than did 60 and 80% TD pellets, while 99% TD pellets exhibited the lowest gas release fraction. Gas release increases with temperature, particularly when 1000°F is exceeded in the pellet irradiations. Analytical calculations of burnup levels in the samples agreed well with values measured by $^{10}B/^{11}B$ isotopic analysis of the powder specimens. Calculations show that difference in sample geometry can cause significant differences in damage distribution due to self shielding. Also, spectral variations between thermal reactors can result in different reaction profiles and damage distribution through a given specimen. These considerations make interpretation of thermal reactor data and extrapolation to performance of B_4C in fast-reactor conditions very difficult, but some of the techniques necessary to do it have been developed during the analysis of this experiment.

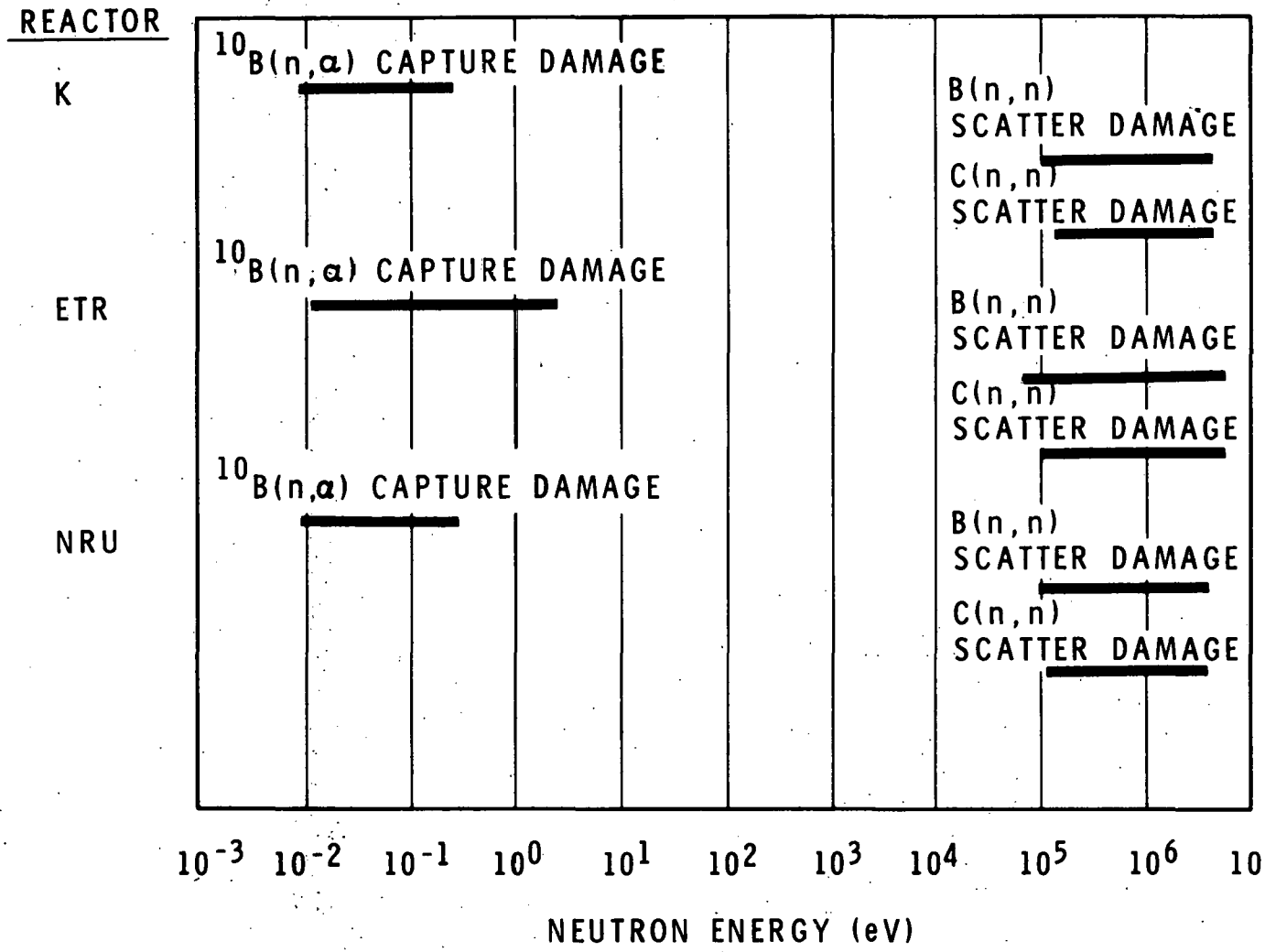

FIGURE 22. B_4C IRRADIATION DAMAGE 90% RESPONSE RANGE FOR TWO MECHANISMS

ACKNOWLEDGMENTS

Capsule design and fabrication was performed by W. E. Hart. The metallography, X-ray, and compatbility testing were performed by L. R. Bunnell of Battelle-Northwest, who also provided interpretation of the results. Through many discussions, Dr. R. E. Dahl has contributed many incisive questions and suggestions to the analysis of this experiment. They have been sincerely appreciated.

REFERENCES

1. W. K. Barney et al. "The Use of Boron Carbide for Reactor Control," Nucl. Sci. and Eng. 1 (1958).

2. R. G. Gray and L. R. Lynam. "Irradiation Behavior of Bulk B_4C and B_4C-SiC Burnable Poison Plates," WAPD-261 (1963).

3. W. D. Valovage. "Effect of Irradiation on Hot Pressed Boron Carbide," KAPL-1403 (1955).

4. D. J. Hamman and P. Schall. "Radiation Effects in Boron Containing Compounds," BMI-1406 (1960).

5. E. W. Hoyt and D. L. Zimmerman. "Radiation Effects in Borides, Part 1, Helium Release and Swelling in Irradiated Borides," GEAP-3743 (1962).

6. Quarterly Progress Report for Period Ending September 30, 1969, "Fuels and Materials Development Program," ORNL-4480.

7. T. Rockwell, III, Ed. Reactor Shielding Design Manual, U. S. Atomic Energy Commission (1956).

8. G. E. Russcher and N. J. Graves. "Computer Codes for Self Absorption Shielding," in preparation.

9. D. R. Secreist. "Compound Formation in the Systems Lithium-Carbon and Lithium-Boron," J. Am. Cer. Soc. 50, 10 (1967).

10. R. E. Dahl, Jr. "Correlation of Radiation Damage in Boronated Graphite," BNWL-199, Battelle-Northwest (1966).

11. R. E. Dahl, Jr. "Preliminary Analysis of Irradiation Tests for FTR Control Material, (Internal Report), Battelle-Northwest (1970).

12. D. R. de Halas. Nuclear Graphite, R. E. Nightingale, ed., Academic Press (1962).

DISTRIBUTION

OFFSITE

No. of Copies	
1	AEC Chicago Patent Group GH Lee, Chief
26	AEC Division of Reactor Development and Technology Director, RDT Asst Dir for Nuclear Safety Analysis & Evaluation Br, RDT:NS Asst Dir for Plant Engrg, RDT Facilities Br, RDT:PE Components Br, RDT:PE Instrumentation & Control Br, RDT:PE Liquid Metal Systems Br, RDT:PE Asst Dir for Program Analysis, RDT Asst Dir for Project Mgmt, RDT Liquid Metals Projects Br, RDT:PM FFTF Project Manager, RDT:RE Asst Dir for Reactor Engrg, RDT Control Mechanisms Br, RDT:RE Core Design Br, RDT:RE (2) Fuel Engineering Br, RDT:RE Fuel Handling Br, RDT:RE Reactor Vessels Br, RDT:RE Coolant Chemistry Br, RDT:RT Fuel Recycle Br, RDT:RT Fuels & Materials Br, RDT:RT Reactor Physics Br, RDT:RE Special Technology Br, RDT:RT Asst Dir for Engrg Standards, RDT LMFBR Program Manager, RDT:PM
1	AEC Idaho Operations Office Nuclear Technology Division CW Bills, Director
1	AEC San Francisco Operations Office Director, Reactor Division

No. of Copies	
5	AEC Site Representatives Argonne National Laboratory - CH Atomics International Westinghouse Electric Corp. General Electric Company Argonne National Laboratory - ID
210	AEC Division of Technical Information Extension
3	Argonne National Laboratory RA Jaross LMFBR Program Office NJ Swanson
1	Atomic Power Development Association Document Librarian
5	Atomics International FFTF Program Office
1	Liquid Metal Engineering Center RW Dickinson
2	Liquid Metal Information Center AE Miller
2	Babcock & Wilcox Company Atomic Energy Division SH Esleeck GB Garton
1	General Electric Co. Nucleonics Laboratory Dr. HW Alter, Mgr. P.O. Box 846 Pleasanton, Calif. 94566
1	Combustion Engineering 1000 MWe Follow-On Study WP Staker, Project Manager
1	Combustion Engineering Mrs. Nell Holder, Librarian
5	General Electric Company Advanced Products Operation Karl Cohen (3)

No. of Copies	
2	Gulf General Atomic Inc. General Atomic Division D Coburn
1	Idaho Nuclear Corporation JA Buckham
2	Oak Ridge National Laboratory WO Harms
1	Stanford University Nuclear Division Division of Mechanical Engrg R Sher
1	United Nuclear Corporation Research and Engineering Center RF DeAngelis
5	Bechtel Corporation JJ Teachnor
10	Westinghouse Electric Corporation Atomic Power Division Advanced Reactor Systems DC Spencer

ONSITE HANFORD

No. of Copies

3 RDT Asst Dir for Pacific Northwest Programs
TA Nemzek

1 AEC Richland Operations Office
JM Shively

1 AEC Chicago Patent Group
RK Sharp (Richland)

1 Battelle Memorial Institute (Columbus)

2 Battelle Northwest
RL Bunnell
BNW Technical Information Files

1 Bechtel Corporation
WA Smith (Richland)

75 WADCO Corporation

DE Baker
MJ Barr
JA Basmajian
TK Bierlein
CA Burgess
JA Christensen
TT Claudson
RE Dahl, Jr.
DG Doran
EA Evans
NJ Graves
WE Hart
JJ Holmes
JE Irvin
JL Jackson
JN Judy
JC Knoll
WN McElroy
AL Pitner (15)
HC Ripfel
WE Roake
WA Ross
GE Russcher (15)
WF Sheely
FR Shober
RL Simons
JW Thornton
JA Ulseth
ET Weber
B Wolfe
HH Yoshikawa
WADCO Document Control (15)
WADCO Tech Pubs